A multi-scale analysis on electrohydrodynamic drying technology for bio-based & food products

Ham, Judith C.A.; Alawi, Aza; Rizki, Zulhaj; Boom, Remko M.; Garbin, Valeria; Padding, Johan T.; Schutyser, Maarten A.I.

DOI
10.1016/j.tifs.2024.104634

Publication date
2024

Document Version
Final published version

Published in
Trends in Food Science and Technology

Trends in Food Science & Technology 151 (2024) 104634

Contents lists available at ScienceDirect

Trends in Food Science & Technology

journal homepage: www.elsevier.com/locate/tifs

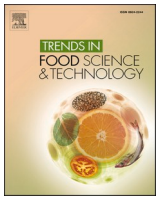

A multi-scale analysis on electrohydrodynamic drying technology for bio-based & food products

Judith C.A. Ham [a,1], Aza Alawi [b,1], Zulhaj Rizki [a], Remko M. Boom [a], Valeria Garbin [b], Johan T. Padding [c], Maarten A.I. Schutyser [a,*]

[a] Food Process Engineering Group, Wageningen University, Bornse Weilanden 9, 6408 WG, Wageningen, the Netherlands
[b] Department of Chemical Engineering, Delft University of Technology, van der Maasweg 9, 2629HZ, Delft, the Netherlands
[c] Department of Process and Energy, Delft University of Technology, Leeghwaterstraat 39, 2628CB, Delft, the Netherlands

ARTICLE INFO

Handling Editor: Dr AR Jambrak

Keywords:
Electrohydrodynamic (EHD) drying
Electrically driven
Corona wind
Electromigration
Electroosmosis
Convective drying

ABSTRACT

Background: Electrohydrodynamic (EHD) drying relies on the generation of a **corona wind** that is created with a high electric potential between an emitter and a ground electrode. The impinging **corona wind** enhances convective heat and mass transport close to the sample, which is positioned on the ground electrode. Although **EHD drying** is reported to have large potential for milder and energy efficient drying, most studies have only evaluated its potential at the lab scale and for specific applications.

Scope and approach: This review focusses on discussing the underlying physical phenomena that may be expected to influence the performance of **EHD drying** processes. Specifically, we discuss how **corona wind** changes due to discharge behaviour as it is influenced by moisture release during drying, how the microstructural properties of the product could influence **electromigration** in the drying material and how **EHD drying** could be efficiently and safely scaled up for biobased & food products. We conclude with an outlook to the research that still is required to concretize the potential of **EHD drying** in practice.

Key findings and conclusions: In EHD drying, electrical discharge induces airflow which enhances external **convective drying**. Studies coupling physical phenomena are still lacking, although some possible couplings are mentioned in chapter 2. Internal mass transfer is enhanced due to presence of an electrical potential over the product, which can cause several **electrically-driven** transport phenomena as discussed in chapter 3. Several drying setups have been explored in industry, of which the characteristics are summarized in chapter 4.

1. Introduction

Drying plays a pivotal role in food and biobased production because of the inherent shelf stability of dry foods and materials and the efficiency for transportation. Many drying processes employ hot air to facilitate water removal from either a liquid formulation or a semi solid slurry. Hot air dryers are on average responsible for 12–20% of the overall energy consumption of a food production process, but can be as high as 40% for example for production of skimmed milk powder (Raghavan et al., 2005). About 35–45% of the energy input is lost during drying, for example via the outlet airflow and dryer walls (g, Tantakitti, & Thavornun, 2008). Drying is a complex process during which not only water is removed but also a microstructured product is obtained, which is a major determinant of its quality. Thermal drying is energy intensive and imposes a relatively high heat load on the product (Lewicki, 2006). Therefore, there is a continuous interest in novel drying methods that operate at lower drying air temperatures and use less energy. Electrohydrodynamic (EHD) drying enhances mass and heat transfer during drying and thus allows water removal at relatively lower drying air temperatures while still achieving similar drying rates (Defraeye & Martynenko, 2018b; Iranshahi, Onwude, Martynenko, & Defraeye, 2022; Martynenko, Astatkie, Riaud, Wells, & Kudra, 2017; Martynenko & Zheng, 2016).

EHD drying involves corona wind generation by electric discharge. Corona wind is generated by applying a large electric potential difference between a sharp emitting electrode area and a grounded surface on which the product to be dried is placed. When the electric field surpasses a certain threshold, a corona discharge occurs by ionization of air

* Corresponding author.
E-mail address: maarten.schutyser@wur.nl (M.A.I. Schutyser).
[1] These Authors contributed equally.

https://doi.org/10.1016/j.tifs.2024.104634
Received 3 May 2024; Received in revised form 28 June 2024; Accepted 10 July 2024
Available online 11 July 2024

molecules close to the small electrode due to a high local electrical field strength. The ions are accelerated by the electric field and collide with other air molecules. This initiates an air flow or ionic drift, commonly referred to as the corona wind (Park, Cvelbar, Choe, & Moon, 2018). By placing a wet product in the path of the ions, the corona wind will impinge on the product and enhance drying (Defraeye & Martynenko, 2018b; Iranshahi, Onwude, Martynenko, & Defraeye, 2022; Martynenko, Astatkie, & Defraeye, 2020).

The use of a corona wind has been extensively studied for various technologies (Park et al., 2018; J. Wang, Zhu, Cai, Zhang, & Wang, 2020). While convective drying exists already since the 19th century (Chandramohan, 2020), the effects of EHD during convective drying is not yet fully understood. Previous EHD drying studies mostly studied its effect on the external (air-side) heat and mass transfer rates. A summary of such studies has been made available in literature such as in the work of Martynenko et al. (Martynenko, Bashkir, & Kudra, 2021). However, the application of an electric field during EHD drying may also influence the mass transfer inside drying products, while the release of moisture into the air may affect the ionic wind generation. These complexities have been mostly neglected until now but are hypothesized to be important in larger-scale EHD drying technology. At the same time, until now EHD has been mostly applied in configurations quite similar to those used in conventional convective drying, but the system configurations have not yet been optimized for EHD as such. This it is important to investigate the different phenomena during EHD, and understand their interactions.

The physical phenomena occurring during EHD drying are summarized in Fig. 1.

One phenomenon that is typically neglected is the influence of the electric field on the internal mass transfer. During EHD drying, food products are placed between the electrodes. The main mechanism for water removal is convective drying which is initially externally limited but at a later stage internally limited as water diffusion in the product is slow (Barbosa-Cánovas & Vega-Mercado, 1996). The corona wind necessitates a (small) ionic current, which also has to pass through the product. The electrical potential drop across the product may influence internal mass transfer and may induce ohmic heating. The electrical potential drop across the product may influence internal mass transfer and may induce ohmic heating. Ohmic heating depends on the electrical potential drop and conductivity, both influenced by the moisture content of the material. Ohmic heating provides volumetric heating of the sample, which indirectly also influences the diffusion of water. The influence of the electric field on the internal mass transfer (either water or charged species) during EHD drying has been mentioned in literature but not studied in detail. Many studies assume that the products are relatively thin (Iranshahi, Onwude, Martynenko, & Defraeye, 2022; Paul & Martynenko, 2022) and thus do not experience a significant electric potential difference. This assumption seems reasonable from a system perspective, as the electric field strength is very high near the discharge electrode and diminishes towards the ground electrode (Adamiak & Atten, 2004; Defraeye & Martynenko, 2018a, 2018b). However, at a closer look, there is still a residual electric potential across the product, which depends, for example, on the electric permittivity, and especially at later stages of drying the electric conductivity will drop, which will increase the potential difference over the product and thus enhance its effect. This could explain the variability of EHD with different types of materials (Defraeye & Martynenko, 2018b). Even though it is not explicitly discussed in the work of Defraeye and Martynenko (Defraeye & Martynenko, 2018a), their model predicts the residual electric potential across a food sample with various permittivity values. A residual electric potential only exists if a sample is not (highly) conductive, which is the case for most food products (Icier & Baysal, 2004; Rezinkina et al., 2017; Tıraş, Dede, & Altay, 2019). This residual electric potential may induce enhanced transport, such as electroosmosis (O'Brien, 1986). Another study clearly showed enhanced drying for food samples located within the electric field compared to samples placed outside the electric field (right below the electrode), even though both were exposed to similar ionic wind speeds (Martynenko et al., 2020). This observation highlights the need for further study into the internal water transport during EHD drying. Click or tap here to enter text. Another study clearly showed enhanced drying for food samples located within the electric field compared to samples placed outside the electric field (right below the electrode), even though both were exposed to similar ionic wind speeds (Martynenko et al., 2020). This observation highlights the need for further study into the internal water transport during EHD drying.

Another phenomenon that is often neglected is the influence of the evaporation on corona wind generation. The water that evaporates from the surface increases the relative humidity in the drying air. This can impact the electric potential due to changing air properties and the corona wind generation being dependent on relative humidity and temperature (J. R. Lee & Lau, 2017; Zeng, Qu, & Zhang, 2023).

This review summarizes our current understanding on the important

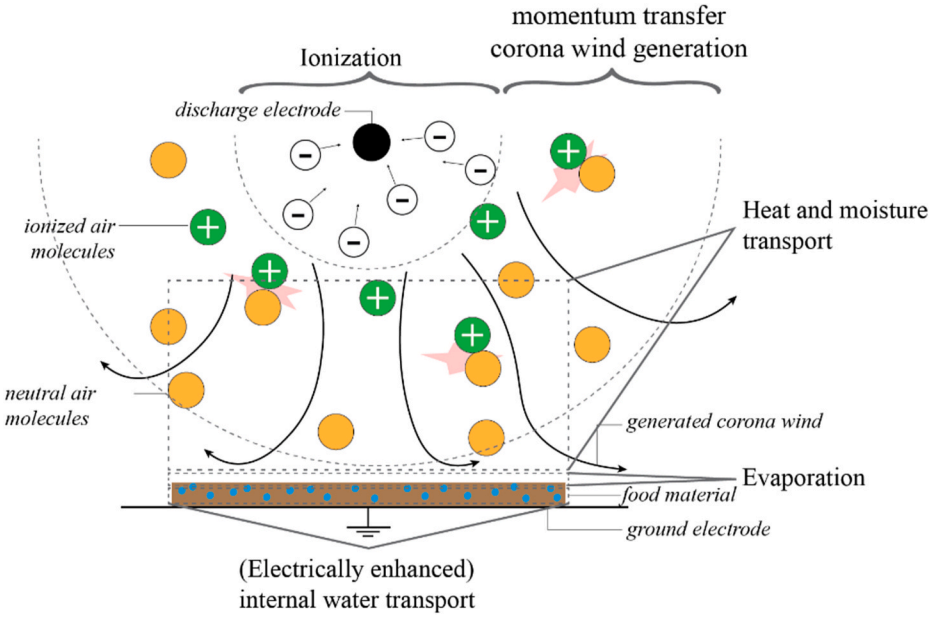

Fig. 1. A schematic description of different energy and mass transport mechanisms in EHD drying.

phenomena during EHD drying and critically discuss the interactions between corona wind generation, external heat and moisture transport and internal moisture transport. In section 2 we focus on the main phenomena related to EHD drying that occur in the air domain including the effect of evaporation on corona wind generation. Subsequently, in section 3 we connect this to the internal transport phenomena during EHD drying including the effect of the electric field on mass transfer inside the product. We then discuss the scalability and safety of EHD (section 4). Finally, we provide an outlook to aspects that we will need to better understand to make EHD suitable for practical application.

2. Air-side heat and mass transfer by corona wind

2.1. Corona wind generation

Corona wind generation involves two stages, i.e. corona discharge and air drift. Corona discharge occurs when air is exposed to a strong electric field, for example around a sharp emitting electrode. The local intense electric field ionizes some air molecules. This phenomenon is well known, and precedes lightning in the air. The extended electric field then accelerates the ions that are created. The drag between these ions and the uncharged air molecules then drags these latter along, generating an air drift (Adamiak & Atten, 2004; Moreau, Audier, & Benard, 2018; Robinson, 2013).

One common approach to model corona wind generation is using a continuum model based on electric current continuity (Defraeye & Martynenko, 2018a; Jewell-Larsen et al., 2008; Onwude, Iranshahi, Rubinetti, Martynenko, & Defraeye, 2021; Park et al., 2018) (eq. (1)).

$$\nabla \bullet \boldsymbol{J} = 0 \tag{1}$$

The electric current is represented as the current density, $\boldsymbol{J}$, generated by the transport of charged species in the air. To date, researchers have identified three potential transport mechanisms, which are expressed in equation (2). Firstly, the transport directly due to the electric field, which is related to the electric field strength, $\boldsymbol{E}$. Secondly, the advective transport due to the air movement, which depends on the air velocity, $\boldsymbol{u}$. Lastly, the diffusive transport due to the charge gradient in the air, $\nabla\rho_e$ (Defraeye & Martynenko, 2018a).

$$\boldsymbol{J} = -\mu_e\rho_e\boldsymbol{E} + \rho_e\boldsymbol{u} - D_i\nabla\rho_e \tag{2}$$

Ion mobility μ_e depends on several environmental variables, such as the polarity of the emitter and the specific ionic species involved. For instance, in the case of air, various ionic forms of oxygen and nitrogen are usually present. Although the formation and transport of these ionic species can be studied in more detail, for EHD applications, commonly a fixed ion mobility is assumed. The value is typically $1.8 - 2.3\ .10^{-4}\ m^2\ V^{-1}\ s^{-1}$ (Adamiak & Atten, 2004; Defraeye & Martynenko, 2018a; Jewell-Larsen et al., 2008). The space charge density in the air domain is determined by the electric potential distribution, which is described by Poisson's equation (Defraeye & Martynenko, 2018a; Jewell-Larsen et al., 2008) (eq. (3)). The distribution is influenced by the relative permittivity, ε_r, which compares the permittivity to that in a vacuum, ε_0.

$$\nabla(\varepsilon_0\varepsilon_r\boldsymbol{E}) = \rho_e \tag{3}$$

with the electric field $\boldsymbol{E}$ defined through

$$\boldsymbol{E} = -\nabla V \tag{4}$$

For the continuity equation, we need to define the space charge density and electric field at the system boundaries, which are situated at both electrodes. Since one of the electrodes is commonly grounded, the main challenge lies at the emitter electrode. One approach to establish this boundary condition is through iterative solving (Defraeye & Martynenko, 2018a; Dumitran, Atten, Notingher, & Dascalescu, 2006) of Poisson's equation (eq. (3)) such that the electric field locally attains the breakdown electric field strength. Assuming a very thin ionization layer (Dumitran et al., 2006; Jewell-Larsen et al., 2008), we can then estimate the local electric field normal to the emitter surface, E_e, using an empirical Peek's – Kapstov's equation (Kaptsov, 1947; Peek, 2017), as expressed in equation (5). In this equation, the empirical constant, γ, is defined as 1 for cylindrical electrodes and 0.1 for spherical electrodes. The emitter radius (r_e) is expressed as a dimensionless quantity, using the value of the emitter radius in centimeters (Adamiak & Atten, 2004). This distinction effectively closes the system of equations, and allows solution of the charge distributions in the EHD drying system.

$$E_e = 3.1 \bullet 10^6 \left(V\,m^{-1}\right)\left(1 + \frac{0.308}{\sqrt{\gamma\, r_e}}\right) \tag{5}$$

The energy transfer from the corona discharge, which creates air drift, can be quantified as an electrical force, $\boldsymbol{F_e}$, and can be integrated into the momentum balance within the Navier-Stokes equation (eq. (6)). In this equation ρ_a is the air density, μ_a is the air dynamic viscosity and ∇p is the pressure gradient.

$$\rho_a\boldsymbol{u} \bullet \nabla\boldsymbol{u} = -\nabla p + \mu_a\nabla^2\boldsymbol{u} + \boldsymbol{F_e} \tag{6}$$

The electrical force on a charged molecule within a continuum consists of three components: the Coulomb force, the dielectric force, and the electrostriction due to the inhomogeneity of the electric field in the medium (Saneewong Na Ayuttaya, Chaktranond, Rattanadecho, & Kreewatcharin, 2012; Taghavi Fadaki, Amanifard, Deylami, & Dolati, 2017). Each component is formulated and summed up to equation (7).

$$\boldsymbol{F_e} = \rho_e\boldsymbol{E} - \frac{\varepsilon_0}{2}|\boldsymbol{E}|^2\nabla\varepsilon_r + \frac{\varepsilon_0}{2}\nabla\left(|\boldsymbol{E}|^2\rho_a\frac{\partial\varepsilon_r}{\partial\rho_a}\right) \tag{7}$$

As alternative to the continuum model, a plasma model can be used to describe the corona wind generation. Air ionization creates a local plasma, being a mixture of charged components (Adhikari & Khanal, 2013; Bittencourt, 2004). The plasma model considers a chain reaction of charged species that can be related to the charge density distribution within the air domain. With such detail of charged species, the plasma model can capture the effect of different gases (although one usually employs air during drying) and the creation of corona wind (Granados, Pinheiro, & Sá, 2016; Mushyam, Rodrigues, & Pascoa, 2019). However, solving the involved system of equations is complicated and this poses a challenge when integrating these with modelling other aspects of the EHD drying process.

2.2. Evaporation and moisture transport

EHD employs corona wind to enhance heat and mass transfer. Heat is transferred convectively via the air and first used to evaporate the water while the product temperature remains constant (constant rate period). After a while, internal moisture transport will become limiting and the product's temperature will increase (falling rate period). During the constant rate period, the heat flux, q, is fully used to evaporate water, and is limited by the finite convective heat transport to the surface. Mathematically, this can be expressed by equating the product of latent heat of evaporation, ΔH_{evap}, and water flux, N_w, to the convective heat transport. The convective heat transport is formulated as the product of the convective heat transfer coefficient, h_a, and temperature gradient between the air, T_a, and the product surface, T_f (eq. (8)).

$$q = N_w\Delta H_{evap} = h_a\left(T_a - T_f\right) \tag{8}$$

Because water is a polar molecule, its evaporation process is affected by the electric field. Evidence of enhanced evaporation by an electric field has been reported in experimental studies (H. Xu et al., 2021; Zheng, Liu, Cheng, & Li, 2011) and in modelling studies (Huang & Lai, 2010; Wu, Xu, Tian, Luo, & Xiong, 2022). These studies demonstrated that the level of enhancement varied depending on the electric field's direction and homogeneity. Specifically, systems featuring a large and

inhomogeneous electric field, characteristic of EHD setups, provided a greater advantage compared to their homogeneous counterparts (Zheng et al., 2011).

Enhanced evaporation occurs due to a lowered activation energy of evaporation (Fei et al., 2021). This implies that the electric field only affects the evaporation kinetics, but not the overall energy needed for evaporation. However, since drying itself is indeed a dynamic process, faster evaporation kinetics may be beneficial.

As water vapor evaporates from the product surface, it enters the air domain. Subsequently, the vapor is transported through the air and finally exits the dryer. Moisture transport through the air involves both diffusion and convection, quantified by a dedicated transport equation (eq. (9)). This equation shows the water vapor accumulation over time, expressed through its mass concentration, C_w, which is determined by its convective (second term) and diffusive (third term) transports, as well as its evaporation rate N_{evap}.

$$\frac{\partial C_w}{\partial t} + \boldsymbol{u} \bullet \nabla C_w + \nabla \bullet \boldsymbol{N}_w = N_{evap} \tag{9}$$

with the diffusive moisture transport described as follow

$$\boldsymbol{N}_w = -D_{w,a} \nabla C_w \tag{10}$$

During EHD, the electric field creates an ionic wind that in turn triggers convective transport of water vapor. Thus, the air velocity, $\boldsymbol{u}$, in equation (9) is coupled to the ionic wind velocity generated in the EHD system (eqs. (2)–(7)).

Further enhancement of moisture transport within the electric field could come from the diffusive part due to the alignment of water molecules. Theoretically, alignment of water molecules in an electric field should occur regardless of its phase. This was confirmed by a recent study (Xie, Hao, Wang, Kou, & Fan, 2022) that reported elevated diffusion rates of water vapor in a gas.

2.3. Coupling between physical phenomena within the air domain

The assumed EHD drying mechanism involves a sequence of the processes discussed in sections 2 and 3; creation of corona wind is followed by drying using this wind. A strong electric field induces a corona discharge. This drives air movement (ionic wind) through momentum exchange between ionized and neutral air molecules (eq. (6)). The ionic wind then enhances surface water evaporation and transfers the water vapor towards the bulk of the air. In laboratory environments, the level of evaporation remains low compared to the amount of available air. However, in larger-scale drying operations, the accumulation of water vapor in the air can impact the corona wind generation and the transfer rates.

It is clear that these effects influence each other. Assuming one-way couplings eases the calculations but will compromise the prediction accuracy. Incorporating two- or multiple-way coupling will enhance the accuracy. These couplings can later be assessed and simplified when they are found to be negligible under the relevant conditions. Possible couplings between phenomena within the air domain are summarized in Fig. 2.

Equation (2) depicts three sources of electric current in EHD systems: (1) electric field-driven, (2) convective transport-driven, and (3) diffusive transport-driven. Diffusive transport is often small compared to their convective equivalent, indicated by relatively small values of diffusivity coefficient, D_i, (Defraeye & Martynenko, 2018a; Jewell-Larsen et al., 2008). This allows us to neglect the third part of equation (2), simplify it to two sources of electrical current.

Convection driven transport of charged species in EHD creates two-way coupling. Air movement is driven by the electric field gradient, while the electric field is also affected by the transport of charged species itself. This implies that equations (2) and (6) have to be solved simultaneously, increasing the computational requirement. A simplification

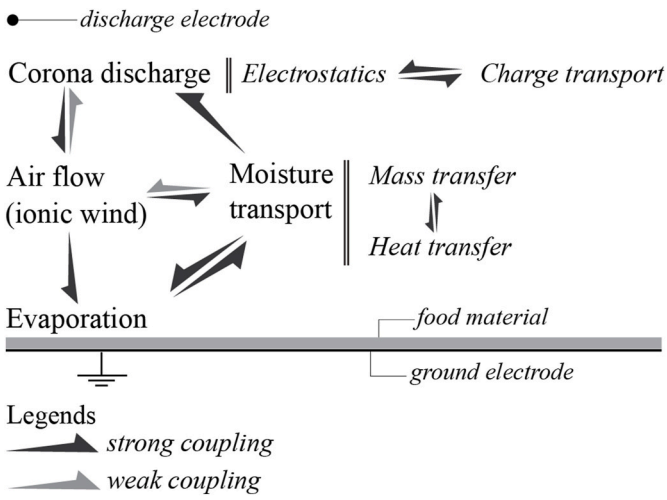

Fig. 2. Diagram illustrating the generation of corona wind, external transport, and the interconnected relationships between these physical phenomena.

of this problem was reported by assuming that the electric field dominates the convective transport (Defraeye & Martynenko, 2018a). This simplifies equation (2) to be solely dependent on its first part.

Evaporation and moisture transport involve the intricately linked mass and heat transfer, as the energy exchange is closely related to the material flow. Within the air domain, convective transport plays a pivotal role, thus, air flow is also coupled to the existing mass and energy balance. In a unidirectional coupling approach, the electrostatics and charge transport affect the moisture transport as it generates the ionic wind. During drying, moisture will accumulate in the air domain as the products are dried. This accumulation should ideally be kept at a minimum, but some moisture build up cannot be completely avoided. This raises the question how humidity influences the electrostatic and charge transport. A moisture-dependent charge transport system gives rise to a complex, multi-directional coupling.

Humidity dependent corona discharge phenomena have been reported (J. R. Lee & Lau, 2017), but the effect of the humidity on the corona discharge has not been well quantified. By reflection on the governing equations (eqs. (1)–(7)), we expect that it will affect the charged species mobility, μ_e.

Actually, earlier EHD studies have not clearly investigated the effect of temperature on corona wind generation, while temperature affects air density and ion mobility and thus wind generation. A physical phenomenon that is often neglected during EHD studies is ohmic heating of the air. A few studies have reported that ohmic heating can specifically enhance heat transfer, albeit more in combination with natural convection rather than with forced convection (Golsefid, Amanifard, Deylami, & Dolati, 2017; Martynenko & Misra, 2021).

In addition to the phenomena occurring in the bulk air that have been explained, there has been limited exploration of the interface and boundary layer. Specifically, the impinging jet configuration creates a boundary layer that differs from the typical one found in most convective drying processes. Furthermore, the counterflow of water vapor from the surface and the presence of ions in the air may locally heat the boundary layer and potentially lead to increased turbulence. This enhanced turbulence could, in turn, reduce the thickness of the boundary layer. The behaviour of ionized air at the interface and its transfer of charge to the sample remain inadequately described. (Golsefid et al., 2017; Martynenko & Misra, 2021). Addressing these gaps is crucial for future research, particularly in the context of large-scale EHD drying processes.

3. Internal moisture transport in materials during EHD drying

3.1. The presence of an electric field in the product during EHD drying

In EHD drying, a product sample is exposed to an electric field, leading to an internal electric field inside the sample. The current generated by the ionic wind also has to pass through the drying material, requiring a certain (ionic) current. Commonly in literature, the improved drying performance in EHD is ascribed exclusively to the increased convection induced by the ionic wind, whereas the effects of the electric field in the drying material are neglected.

A first step was taken by Iranshahi et al. with a study towards understanding the additional contribution of this electric field for water removal experimentally (Iranshahi, Onwude, Martynenko, & Defraeye, 2022). In their experiment, the effect of the electric field was decoupled from the effects of convection by placing the sample at different positions with respect to the ground electrode (see Fig. 3a). The material present in the electric field showed a higher drying rate compared to the sample just below the grounded mesh, as seen in Fig. 3b. This suggests that the electric field in the sample also benefits the internal mass transfer during EHD drying, although the dominant transport mechanism remains to be established. In addition there could be an effect of the migration of the ions through the boundary layer as well.

Iranshahi et al. compared theoretically the contributions of electro-osmotic and electrocapillary flow relative to external mass transfer for drying of foods (Iranshahi, Onwude, Martynenko, & Defraeye, 2022). During the constant rate drying period, the flux of water through one cylindrical pore or from one single cell was estimated in the range of $10^{-6} - 10^{-3}\ kg \bullet s^{-1} \bullet m^{-2}$ for electroosmotic flow and for electro- and thermocapillary flow, whereas the convective flux to air was found to be in the order of $10^{-2}\ kg \bullet s^{-1} \bullet m^{-2}$. This suggests that also during EHD drying is dominated by convection during the constant rate period. At the same time, a positive effect of the electric field was observed in experiments compared to the control (Ding, Lu, & Song, 2015; Taghian Dinani, Havet, Hamdami, & Shahedi, 2014).

The exact effects of electrohydrodynamics on drying is not always clear. For example, in one study, the drying curves of oven-dried samples overlapped with those of EHD dried samples for the entire drying period (Esehaghbeygi & Basiry, 2011). In another study, hot-air dryers still outperformed EHD, which could be attributed to the absence of any enhancement by the ionic wind and/or electric field for their particular operating conditions (Iranshahi, Onwude, Rubinetti, Martynenko, & Defraeye, 2022). These observations imply a knowledge gap with regard to the operating window in which EHD drying enhances water removal. This may be mitigated by elucidating the relation between water removal to internal electrically induced transport, considering sample properties (structural and chemical) and process conditions.

3.2. Internal mass transfer during drying can be affected by an electric field

To better understand the relation between process conditions and material for EHD drying, Bashkir et al. reviewed and compared experimental EHD drying conditions and results in the same metrics (Bashkir, Defraeye, Kudra, & Martynenko, 2020). Earlier EHD drying studies used a variety of conditions and mainly collected empirical data. Most studies reported specifically the drying rate and moisture content evolution for only an initial period of drying (Alemrajabi, Rezaee, Mirhosseini, & Esehaghbeygi, 2012; Esehaghbeygi, 2012). A first step towards better understanding of the internal transport induced by EHD is to consider the different water transport mechanisms in different material types such as solutions, suspensions and (semi-)solids. Hitherto, most EHD studies focused on drying semi-solid materials such as fruits and vegetables (Suvanjumrat, Chuckpaiwong, Chookaew, & Priyadumkol, 2024; Y. Wang & Ding, 2023), while studies on EHD drying of solutions and suspensions highly relevant to food industries are scarcely reported. The physical nature of the different matrices may be expected to have significant influence on the internal mass transfer phenomena which also are potentially influenced by the presence of an electric field. Depending on the matrix properties, a porous structure may already exist or may gradually develop during drying (see Fig. 4). The presence or development of porosity or other forms of inhomogeneity will have profound effect on the transport mechanisms in the materials.

The production of many food ingredients is based on wet extraction from biomass followed by a concentration and drying step (Sridhar, Vaishampayan, Senthil Kumar, Ponnuchamy, & Kapoor, 2022). Generally, first a concentration step (e.g. by evaporation, membrane separation or pressing) is applied, followed by a final drying step. The drying step transforms a (viscous) suspension or slurry into a dried powder. During convective drying of well-soluble food ingredients (such as for example maltodextrins or proteins) the material will develop a gradient in density and consistency which can lead to internal porosity, as shrinkage of the dried structure is prevented by the locally viscoelastic matrix (Moučka, Sedlačík, & Pátíková, 2023). Suspensions of fibres are usually preconcentrated by pressing into a cake. During drying, macroscopic porosity will develop since the initially interstitial water

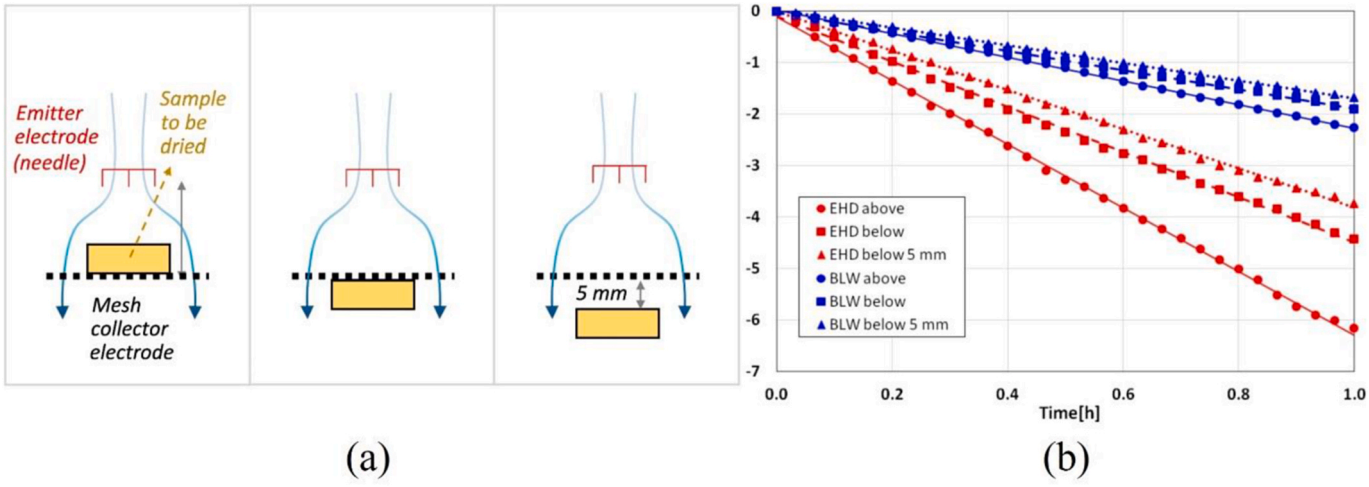

Fig. 3. The effect of residual electric field on drying during EHD (Martynenko et al., 2020). a) The effect of the residual electric field is decoupled from the convective flow by placing the sample at different positions with respect to the electrode. b) Sample is exposed to an electric field and convection has a higher drying rate (see EHD above).

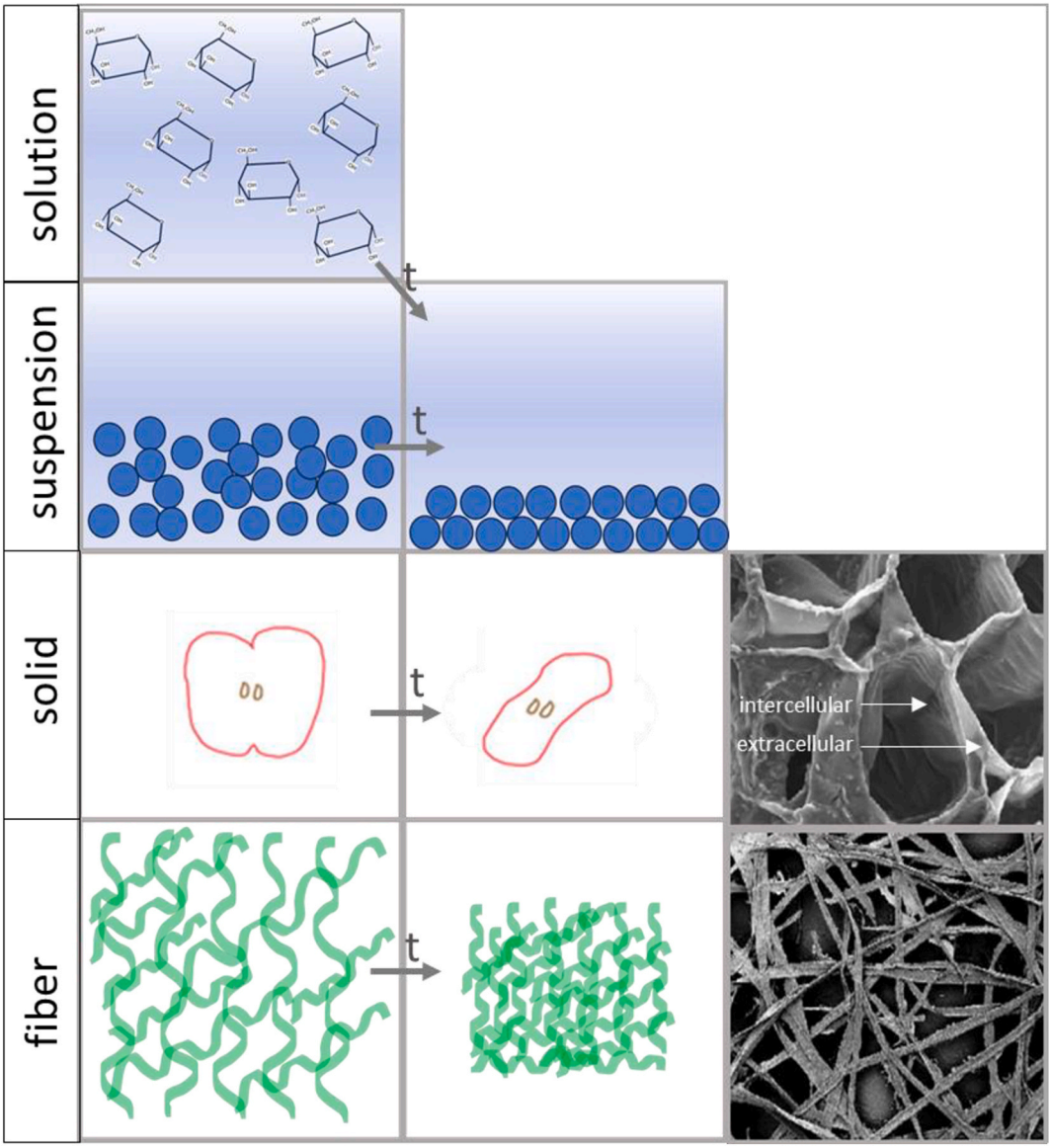

Fig. 4. Solutions, suspensions, solid and fibres undergo structural changes during drying. This leads to the formation of a (more) porous matrix after time t. The micro-structure images of solid and fibre are respectively adapted from (Frabetti et al., 2023) and (C. Liu, Yu, Kirk, & Xu, 2016), respectively.

between the solid particles is removed. In a second stage, the water present within the suspended fibres will be removed during drying, which is limited by internal diffusion. Many food slurries and types of biomass will be in between fibres and dissolved materials, and therefore will experience similar phenomena.

Organic matter typically has a surface charge and therefore counterions are present in water (Alberts et al., 2015). These ions migrate together with their hydration shell under the influence of an electric field, which may enhance or reduce the net migration of water, depending on the sign of their charge. Understanding how charged species in matrices respond when exposed to an electric field and how structural properties affect migration of water for different types of materials can help the development of more effective EHD.

3.3. Electrically driven water transport mechanisms

This section elaborates on different electrically-induced transport mechanisms that may play a role during EHD drying. The phenomena of electro-osmosis, electro-capillary flow, thermocapillary flow and electroporation might be dominant during the falling rate period (Fig. 5). All materials will end up being porous to some extent, therefore in all matrices mentioned in section 3.2 similar transport mechanisms can play a role in the falling rate period.

1. *Electro-osmosis*

An electro-osmotic flow (EOF) requires the presence of a charged surface and an electrolyte solution. Most organic matter is negatively charged, with tightly adhered positive counterions close to the surface due to coulombic forces in the Stern layer. The adjacent, more diffuse Debye layer holds a surplus of mobile positive ions that are more mobile. This region has a thickness in the range of 1–100 nm, depending on the ionic strength (Stone, Stroock, & Ajdari, 2004). When exposed to an external electric field, these excess charges move under the influence of the electrostatic forces and will exert viscous drag on the neutral bulk fluid, resulting in migration of the water.

EOF occurs in porous materials with pore sizes smaller than about 100 μm. The velocity of the liquid due to EOF is described by the Helmholtz-Smoluchowski equation:

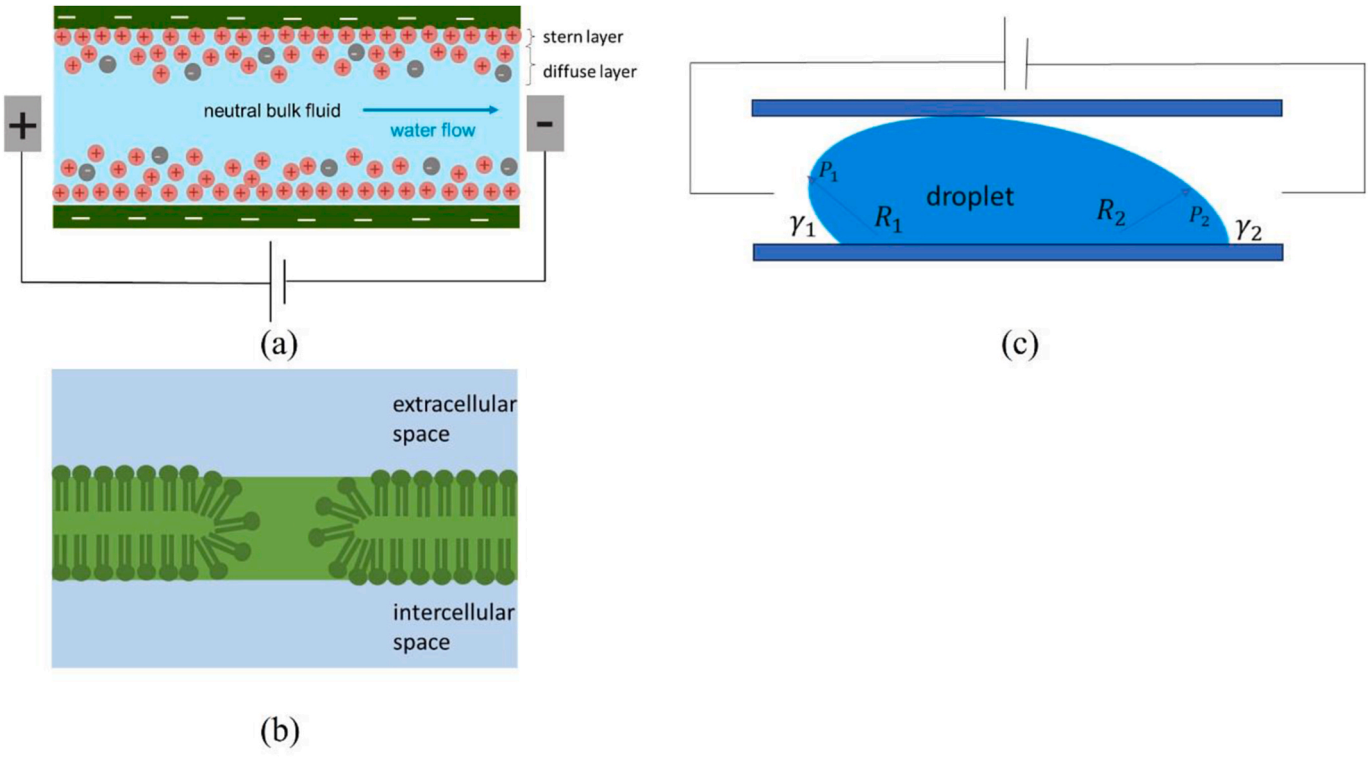

Fig. 5. Electrically-induced water transport mechanisms. a) Schematic of electro-osmotic flow (Wall, 2010). b) Schematic of pore formation in a cell membrane (Golberg & Rubinsky, 2013). c) Droplet flow due to the change in surface tension across the droplet (X. Xu et al., 2018).

$$\boldsymbol{u} = \frac{\epsilon_r \zeta}{\mu} E_{\parallel} \tag{11}$$

Where ε_r is the relative permittivity of the fluid, ζ the zeta-potential of the pore wall, μ the fluid's viscosity and $E_{\parallel}$ the electric field parallel the pore wall (Wall, 2010). It can be estimated that the electric field inside the sample is sufficiently strong for EOF to be relevant during EHD drying. If we assume for simplicity that the emitting and ground electrode are parallel plates, the total electric potential V between emitting and ground electrodes is the sum of the electric potential across the sample and the air:

$$V = E_{\perp s} d + E_{\perp \mathrm{air}} L \tag{12}$$

with d the sample thickness, L is the distance between the emitting electrode and the sample, $E_{\perp s}$ the perpendicular component of the electric field strength inside the sample and $E_{\perp \mathrm{air}}$ is the perpendicular component of the electric field in the air. Further assuming that the sample-air interface itself carries negligible charge, the electric displacement in the sample ($D_{\perp s}$) and air ($D_{\perp \mathrm{air}}$) must be equal, and $E_{\perp \mathrm{air}}$ can be rewritten in terms of $E_{\perp s}$ using equations (13) and (14), where ϵ_0 is the vacuum permittivity, and ϵ_s is the permittivity of the sample.

$$D_{\perp \mathrm{air}} = D_{\perp s} = const. \tag{13}$$

$$\epsilon_0 E_{\mathrm{air}} = \epsilon_0 \epsilon_s E_{\perp s} \tag{14}$$

Eq. (15) shows that the electric field inside the sample is only ϵ_s times smaller than that in the air. The above equations can also be used to estimate the potential at the sample-air interface, V_{interf}, relative to the total electric potential V:

$$\frac{V_{interf}}{V} \approx \frac{1}{\epsilon_s} \frac{d}{L} \tag{15}$$

Assuming the permittivity of the sample to range between 2 for a very dry material to 80 for a very wet material and the applied voltage to be 10 kV, V_{interf} can be calculated to be 1–1000 V depending on the thickness of the sample. These results show that the electric field and voltage across the sample can be sufficient to induce EOF in a pore.

EOF has been widely studied for dewatering of soil and sludges. Due to the similarities between soil and biomass, insights in this field may be translated to dewatering of biomass. For example, the effect of sample thickness (J. Liu, Wu, Zhou, Liu, & Wei, 2022), electric field (C. Xu et al., 2023), and electrolyte (Li, Yu, Zhang, & Zhang, 2021) on the effectivity of electroosmotic dewatering has been the focus of investigation. In general, one finds an optimum ionic strength, whereby an excess of salt will result in the decrease of electric double layer thickness and the reduction of EOF (Gargano, Lirer, & Flora, 2022). This optimum depends on the physiochemical properties of the material. The nature of the solids will co-determine the surface adsorption of ions, while the valency and atomic mass of the ions influence the zeta potential and mobility of the ions respectively, and thus the dewatering by EOF (Gargano et al., 2022) ohmic heating due to the electrical resistance reduces the viscosity and as a result increases dewatering (Zhang et al., 2022). This effect may be important in biological materials, as these tend to become glassy at low water contents and lower temperatures.

A limiting phenomenon for EOF is the depletion of water on one side of the sample. This reduces electrical conductivity and stops EOF. However, due to mechanical or thermal effects, moisture may be redistributed again more homogeneously over the entire sample extending the period during which EOF is possible for dewatering. Redistribution of moisture due to mechanical stresses was for example observed during convective drying of broccoli stems during convective air drying (Jin et al., 2012). Di Fraia et al. reviewed modelling approaches to electroosmotic flow in porous media and concluded that high porosity enhances EOF, while tortuosity decreases it (Di Fraia, Massarotti, & Nithiarasu, 2018). However, experimental validation of this phenomenon is challenging due to incomparable material properties and operating conditions.

2. Electrocapillary flow

Electro-capillary flow of a liquid droplet trapped inside a pore can be induced when an electric field is applied tangentially to an electrically charged pore wall, leading to a difference in the local surface tension at the different locations of the droplet menisci (J. Lee & Chang-Jin Kim, 2000). The change in the surface tension can be described by the Young-Lippman equation, where γ_{SL}, is the droplet surface tension at the solid-liquid interface, C is the electric double layer capacitance, γ_0 is the surface tension when no electric field is applied and V_{wall} the local voltage on the pore wall at the location of the meniscus (Chakraborty, 2008).

$$\gamma_{SL} = \gamma_0 - \frac{1}{2} C V_{wall}^2 \tag{16}$$

The change in surface tension will induce a pressure difference arise across the droplet because of the change in radius of curvature in the advancing and receding part of the droplet, caused by the γ_{SL} gradient (X. Xu, Zhang, & Sun, 2018). This pressure difference as function of the difference in the radii of curvatures is described via the Young-Laplace equation for the advancing part and receding part, with P_{adv} the pressure at the advancing part, P_{rec} the pressure at the receding part, R_1 the radius of curvature at advancing part, R_2 the radius of curvature at receding part and γ_{gl} the liquid-gas interfacial tension:

$$P_{adv} - P_{rec} = \gamma_{gl} \left(\frac{2}{R_1} - \frac{2}{R_2} \right) \tag{17}$$

The electric fields expected in EHD may be sufficient to induce electrocapillary flow in biomass. The electric double layer capacitance is of the order of 10^{-2} Fm^{-2} and water-biomass surface tension is even lower than water-air surface tension (0.072 Jm^{-2}) due to the hydrophilic nature of biomass (Lillard & Pint, 2020). Thus, an electric potential difference of only 1 V across the length of a droplet would be enough to cause a significant change in water-biomass surface tension and hence an electrocapillary flow might be generated. In later stages of drying, it is supposed that individual droplets of water will be present in the material, whereby a two-phase system of water and gas is present. It is hypothesized that this mechanism will be most relevant at that stage.

As can be seen from equation (17), the pressure difference on a droplet depends on the local meniscus curvature of the droplet. Generally speaking, higher curvature menisci are expected in more narrow pores. However, the actual difference in curvature between the two menisci of a droplet will not only depend on the pore geometry, but also on the length and orientation of the droplet relative to the electric field because that determines the difference in local electric potential. Besides, a higher wettability of the droplet on the material, will hamper the flow due to its affinity with the material. Wetting of the droplet is controlled by the surface properties of the material to be dried and the content of the water droplet. Equation (16) shows that the induced surface tension depends on the capacitance of the EDL. The capacitance of an electric double layer is not only affected by ions, but may also depends on the applied voltage (Shrotriya & Yang, 2005).

3. Electroporation

Electroporation of cells is a phenomenon that can be induced by applying a very high electrical potential (Golberg & Rubinsky, 2013). Cell membranes consist of a phospholipid bilayer, which is approximately ~7 nm thick (Rubinsky, Onik, & Mikus, 2007). Upon application of a critical electric field strength, the cell membrane can be disrupted and pores are created. Electroporation has also been applied in combination with drying processes (then also often referred to as pulsed electric field treatment). Electroporation not only creates permeability, but can also facilitate passage of water(-soluble) matter across the membrane (Vaessen, den Besten, Leito, & Schutyser, 2020). Improved drying rates have been observed for cells treated with electroporation (Iranshahi, Onwude, Rubinetti, et al., 2022). The potential across the cell membrane (V_m) as a function of the applied voltage is given by the Schwan's equation, where E is the magnitude of the external electric field $\boldsymbol{E}$, r the cell radius and θ is the angle between the point of interest on a cell membrane and $\boldsymbol{E}$ (Golberg & Rubinsky, 2013):

$$V_m = \frac{3}{2} E r \cos\theta \tag{18}$$

The minimum electric potential difference across a cell membrane required to electroporate it is between 0.2 and 1 V (Golberg & Rubinsky, 2013). This means that an electric field of approximately 1000 kV m^{-1} is required for a cell radius of 1 μm, which is far higher than can be obtained in EHD. Hence, electroporation is not expected to enhance the internal water transport.

4. Thermo-capillary flow

During EHD drying, the temperature of the product will change and on top of that local ohmic heating can occur depending on the electrical potential and the electrical resistance of the material (Martynenko & Misra, 2021). The local temperature of the sample along the thickness may vary during heating depending on the thermal conductivity and thickness of the sample. A gradient in surface tension may then occur as a consequence of the temperature gradient, which gives rise to thermocapillary flow. A change in temperature also lowers the viscosity, which may also enhance dewatering. The surface tension gradient $\Delta\gamma$ as function of temperature gradient Δ T across an individual droplet can be described by (Glockner & Naterer, 2006):

$$\Delta\gamma = -0.1477 \times 10^{-3} \ \Delta T \tag{19}$$

From the above equation it is evident that small temperature gradients already lead to a gradient in surface tension, which may lead to thermo-capillary flow. Once the material becomes dryer, ohmic heating will become more significant as the conductivity decreases. Therefore, thermo-capillary flow might play an important role for water removal from low moisture materials.

4. EHD drying equipment

In this section we discuss EHD equipment design aspects and how environmental factors influence ionic wind generation and drying. Moreover, scale-up is discussed as well as safety issues that should be considered when applying EHD drying at a larger scale.

4.1. Electrode design in EHD equipment

During EHD drying, a discharge is generated between an emitter and collector electrode which generates a substantial electric field and wind velocities which can be employed in drying, as explained before. The wind generation largely depends on the current distribution determined by the emitter-collector configuration and the applied electrical potential. For the relation between current and potential, often the Warburg relation is used (eq. (20)) although for pin-to-plate configurations this equation was found to be only valid for low currents (I < 250 μA) or voltages (V < twice the onset voltage V_0). The Stuetzer model (eq. (21)) is overall more accurate (Martynenko & Kudra, 2020; Stuetzer, 1959). Both depend on a geometrical constant g (1/m), the dielectric permittivity of a vacuum ε_0 (F/m), the ion mobility μ_e ($m^2/V/s$) and the onset voltage V_0 (V). The onset voltage is the minimum potential needed to initiate a current over the electrode gap.

$$I = g\varepsilon_0\mu_e V(V - V_0) \tag{20}$$

$$I = g\varepsilon_0\mu_e (V - V_0)^2 \tag{21}$$

As the dielectric permittivity is a constant and ion mobility an environmental factor, EHD equipment studies focus mostly on design of the emitter and collector electrode to optimize g. However, the influence of environmental factors is also considered (see section 4.2).

Typically, the emitter electrode consists of a needle or wire and sometimes a secondary emitter electrode is added below the primary emitter to enhance airflow (Chang, Peng, Lin, & Lai, 2020). Needle electrodes generate a jet-shaped corona wind while wire electrodes create slot-shaped corona wind (Fig. 6). For scaling up, multiple emitter electrodes can be placed next to each other to cover a larger drying area. Wire electrodes are easily drawn over a large area (Lai, 2010), while multiple-needle systems are found less sensitive to dust collection, which may stabilize the performance over time. Martynenko et al. compared energy efficiencies for EHD drying of different foods in varying setups (Martynenko et al., 2021), and concluded that wires and needles are equally efficient emitters, but that direct comparison is hard because of the difference in applied experimental conditions. It is however observed that single emitter systems have a higher energy efficiency, although they are inefficient compared to multiple-emitter systems for drying large surfaces (Lai & Sharma, 2005; Leu, Jang, & Wu, 2020). Overall, energy efficiency of the system can be improved significantly when optimizing emitter shape (Rubinetti et al., 2024).

Only multi-emitter systems are considered for scale-up towards industrial drying. Additionally, it is important to combine EHD drying with another type of drying to achieve drying rates that are relevant for industrial drying processes. For conductive drying, another electrically enhancing technique, dielectrophoretic drying, was suggested to be more suitable than EHD drying (Yang & Yagoobi, 2022). Therefore, the most logical application of EHD enhanced thermal drying at industrial scale would be in a continuous convective process, such as belt drying with a grounded belt and multiple emitters.

Increasing the emitter spacing (i.e. the space between emitter electrodes) in a multiple emitter system leads to a decrease of the average ionic windspeed at the sample surface and thus a reduced drying rate, for example shown for Chinese wolfberry fruits (Ni et al., 2019). Therefore, Ni et al. suggested minimizing the electrode spacing, but in drying a slurry of probiotics neither the drying rate nor the cell viability was influenced by this closer electrode spacing (Dima, Gulbinas, Stubbe, Mendes, & Chronakis, 2022) and in drying of a film of an amoxicillin solution, a lower emitter spacing even decreased the drying rate (Nicholas & Abuzairi, 2019). It is therefore suggested that decreasing the emitter spacing is useful to increase wind velocity for mass transfer enhancement until a certain optimum, after which the corona jets of different electrodes interfere and humidity will build up in the air (Martynenko & Kudra, 2020).

As a collector electrode, either a plate or mesh can be used. By using a mesh collector, fruit samples were observed to dry faster and more uniform since the product is more exposed to the air, while in an emitter-to-plate set-up the drying only occurs at the top surface. A plate collector electrode surface limits the available area for mass transfer and also the humidified air can less easily be removed from the system (Fig. 6) (Iranshahi, Onwude, Rubinetti, et al., 2022). A mesh electrode design can be further tuned for its performance than a plate electrode, by adjusting the number of grounded wires and non-grounded wires, the position of wires relative to each other and relative to the sample (Iranshahi, Martynenko, & Defraeye, 2020). Additionally, mesh collectors are more easily scalable as a repeatable modular design. However, some products such as pulp or powders cannot be dried on a mesh as they are not self-supporting. These products can either be dried by using a plate collector or a tray of insulating material on top of a mesh, although the effect of the presence of an insulating material between the product and the mesh is unknown. When upscaling these systems, it is harder to control RH by disposal of moist air compared to mesh systems where moisture can be disposed of in between the sample. The efficiency of upscaling of these systems is therefore limited by the path length the generated wind needs to pass to leave the system, as a larger plate means

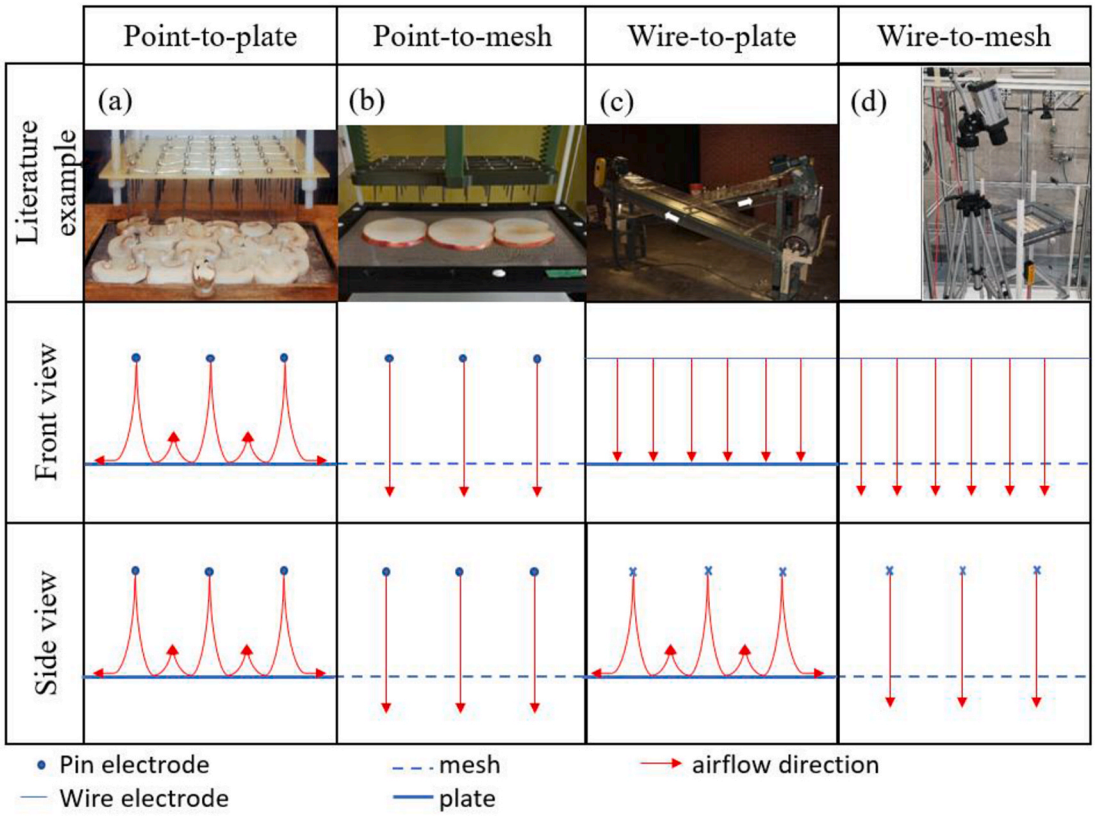

Fig. 6. Examples from literature: a. (Martynenko et al., 2019), b. (Martynenko, Iranshahi, & Defraeye, 2022), c. (Lai, 2010), and d. (Iranshahi, Onwude, Rubinetti, et al., 2022) of different electrode configurations applied for EHD drying, and the schematic overview. Blue lines represent electrodes (dashed lines represent mesh electrodes) and red arrows represent airflow direction. (For interpretation of the references to colour in this figure legend, the reader is referred to the Web version of this article.)

more moisture buildup and that may result in a smaller driving force for mass transfer if no counter measures are taken against RH increase.

Environmental factors such as relative humidity buildup also influence electrical current distribution by affecting ion mobility and dielectric permittivity. Although most studies focus on optimizing electrode configuration for equipment design, it is important to also study design solutions for environmental limitations for equipment (Lai, 2010).

4.2. Process conditions: convection, temperature and relative humidity

For a continuous EHD system, Lai found that an additional cross airflow generated by movement of the product on conveyor belts affected the impinging EHD wind (Lai, 2010), which corresponds with the observation that imposed cross airflow limits the contribution of EHD kinetics to drying (Martynenko & Zheng, 2016). To assess the combined effect of the impinging EHD airflow and a cross airflow, a dimensionless EHD number N_{EHD} was introduced representing the ratio of the electric body force to the inertial force of the cross-flow (eq. (22)) (Lai & Lai, 2007) or the effective EHD air velocity u_{EHD} (m/s) relative to the crossflow air velocity u (m/s). The EHD flowrate is determined by the electrical current I (A), distance between electrodes d_{ec} (cm), density of the air ρ_a (kg/m^3), ion mobility of air μ_e (m^2/V/s) and surface of the collector electrode A (m^2) (Lai & Sharma, 2005). For an EHD number higher or equal to 1, the EHD mechanism roughly dominates drying while below 1, the cross air flow dominates drying.

$$N_{EHD} = \frac{u_{EHD}}{u_a} = \frac{1}{u_a}\sqrt{\frac{Id_{ec}}{\rho_a A \mu_e}} \tag{22}$$

A high EHD number can be reached at either low cross flow or at high EHD air velocities. Additional crossflow is unavoidable when using conveyor belts and can even be beneficial as it was shown that movement of product relative to the emitter improves the homogeneity of drying (Dima et al., 2022). When the sample is not moved on a conveyor belt and no additional crossflow is applied, drying is not homogeneous as the sample is exposed to high wind velocities directly below the emitter compared to further away from the emitter. Because of this, materials are most sensitive to changes in colour and structure directly below the emitter (Dima et al., 2022; Meng et al., 2022).

The ionic wind velocity during EHD can be influenced by changing process conditions such as the temperature and RH, by optimizing equipment design, or by applying higher voltages. For design optimization, the velocity of a jet should be considered in three dimensions of which not necessarily all dimensions are effective in drying enhancement. For example, placing wires perpendicular to the airflow instead of parallel was found to result in higher drying rates under similar conditions, therefore requiring less power per unit water removed (Bardy, Manai, Havet, & Rouaud, 2016). Also the position of a wire electrode relative to the material placed in an additional crossflow was found to be of influence on the airflow direction and thus on convective mass transport (Babaei, Heidarinejad, & Pasdarshahri, 2018). So although the N_{EHD} is useful to compare performance of one EHD system at different process conditions, it is important to consider the effective air flow when comparing different EHD dryer configurations.

Apart from the geometry of the equipment, it is also possible to improve environmental factors to increase wind velocity. Accumulation of humidity in the air was observed in a pilot scale EHD system with wires mounted on walls (Lai, 2010). A high RH negatively affects drying due to lower mass transfer of moisture from the sample to the air and affects EHD drying due to the lower ion mobility at higher RH leading to lower wind speeds (Lai, 2010; Martynenko, Bashkir, & Kudra, 2019). The presence of walls on the side of the plate collector in the pilot set up prevented replacement of the humidified air by drier air. This should be prevented by better dryer design. The inlet air may be hot to further reduce the RH and the air may be applied with (Bardy et al., 2016) or without (Meng et al., 2022) introducing an additional crossflow. Applying EHD during hot air drying enhances the drying rate, with an increased effect at higher electric field strength (Cao, Nishiyama, & Koide, 2004; Meng et al., 2022). The higher drying rates also allowed for reduced running time of the dryer, resulting in an overall lower specific energy consumption (SEC, kJ/kg) for EHD-assisted hot air drying compared to regular hot air drying, despite requiring energy to create the corona discharge (Meng et al., 2022; Taghian Dinani et al., 2014). Further, samples exposed to EHD-assisted hot air drying experienced lower surface temperature, which led to less shrinkage and better rehydration of structured foods (Alemrajabi et al., 2012; Martynenko & Misra, 2021).

Temperature increase itself does not impact the corona discharge behaviour but does accelerate the charge transfer and thus the ionic wind production by reducing the RH (J. R. Lee & Lau, 2017). For the combination of hot air drying and EHD, no additional effect on the drying rate was found beyond a critical high temperature (Cao et al., 2004). Most studies focus on EHD drying at low or ambient drying temperatures where drying rates can be expected to increase more with application of EHD. However, one may expect that an EHD process with higher temperatures will attain industrially relevant drying rates more easily. It remains to be investigated to what extent EHD can still be beneficial at elevated hot air temperatures. Finally, adoption of EHD technology for convective drying processes may also be expected faster if it can be implemented in existing dryer designs.

4.3. Scale-up and safety of EHD dryers

For batch EHD drying, studies have been done on increasing capacity, which may be achieved by either increasing sample thickness (cm) or by increasing loading density on the belt (kg/m^2). Similar to conventional air drying, for EHD drying of apple or strawberry slices an increase in slice thickness resulted in a longer drying time and higher SEC (Paul, Astatkie, & Martynenko, 2022) due to internal transport becoming more limiting. Increasing loading density affects moisture transfer from the surface of materials to the air and thus affecting the constant rate period, also increasing the drying time. However, the overall SEC decreases (Iranshahi, Onwude, Rubinetti, et al., 2022; Onwude et al., 2021; Paul & Martynenko, 2022).

Safety is essential for any process employing large electric potential differences. Increasing the loading density may require higher wind velocities, and higher corona currents. However, the ozone concentration will increase close to the wire when operating at higher current or higher wire radius (Chen & Davidson, 2002; Y. Lee, Kim, Han, Kim, & Kim, 2022; J. Wang, Cai, Zhu, & Liu, 2022), as during corona discharge ozone and nitrogen oxides are generated as by-product. There is no study yet quantifying the ozone production during long drying cycles or using larger scale equipment. For lab-scale equipment using a wire-to-plate configuration (T_a = 300 K, I = 2.55 μA/cm, wire radius = 100 μm) maximum concentrations of 5.8 ppm ozone and 0.028 ppm N_2O were produced very close to the wire (Chen & Davidson, 2002), which was above the recommended 8h threshold of 60 ppb and 21 ppb (European Commission, 2017). However, these local concentrations were only found close to the emitting electrode, and not in the bulk air due to the mixing effect of the generated ionic wind (Chen & Davidson, 2002). The mixing effect of the ionic wind reduced the ozone level below the maximum threshold and the N_2O level to become negligible. Higher ozone and N_2O concentrations might be expected when using a larger wire diameter, possibly relevant for sturdy equipment in an industrial environment. However, the generation of oxidants can be limited by using either a dielectric film coating on top of the collector electrode (Y. Lee et al., 2022), or by applying a magnetic field along the electric field to reduce the current while maintaining high ionic wind velocities (J. Wang et al., 2022).

5. Conclusion and outlook

EHD drying phenomena have been widely studied individually, but it is not yet fully understood how different phenomena influence each other. By producing a corona wind, mass transfer from the surface of the product to the air is enhanced, affecting the constant rate drying. Additionally, internal mass transfer is enhanced due to the presence of an electrical potential over the product thickness, although the extent of this potential is expected dependent on amongst others the moisture content. In this review several electrically-induced transport phenomena are discussed, which may explain an additional benefit for EHD drying beyond only affecting external convective transfer.

Current EHD studies vary in experimental setup, are applied to a range of different sample types and report on different properties, which makes them hard to compare. Often, experiments report only on an initial constant rate period and exclude drying in the falling rate regime resulting in limited information on internal transport limitations of different materials. Based on studies performed in the convection limited drying regime it can be concluded that EHD dryer design should take optimal relative humidity, electrical current and wind generation into account. To find an optimal RH requires more understanding of the underlying relations between humidity, corona discharge and current generation on which little is reported yet. Optimal electrical current and wind velocities are expected to change over time due to changing conductivity of a drying product. However, no time or water content dependent studies of wind velocity and current are available, again neglecting EHD drying in the falling rate regime. Equipment could potentially vary current and wind velocity over time by applying different electric potentials or adapting distance between electrodes during a drying cycle. Similar to the moisture content of the product affecting the electrical current, it is also expected to affect the residual electrical field over the product. As the internal electric field strength varies during the process, it is to be expected that also the governing internal transport mechanisms might vary. However, there are no studies on this topic yet, and little tools are available to track mobility of small components in samples within strong electric fields. Visualization of internal mass transport in EHD drying could prove electromigration mechanisms depending on the material matrix properties. For this, a more systematic approach using model systems and controlled conditions could be used.

EHD drying studies indicate several advantages of EHD over conventional hot air drying in terms of product quality and energy consumption. By utilizing electricity as the primary energy source, EHD drying could enable adoption of renewable energy, such as solar or wind power. However, underlying mechanisms for EHD are still poorly understood and no scalable devices are yet available. Research should be done to pave the way for rational design of efficient and large-scale EHD dryer designs.

CRediT authorship contribution statement

Judith C.A. Ham: conceptualization, writing – original draft, writing – review & editing. Aza Alawi: conceptualization, writing – original draft, writing – review & editing. Zulhaj Rizki: conceptualization, writing – original draft, writing – review & editing. Remko Boom: conceptualization, writing – review & editing, supervision. Valeria Garbin: conceptualization, writing – review & editing, supervision. Johan T. Padding: conceptualization, writing – review & editing, supervision. Maarten A.I. Schutyser: conceptualization, writing – review & editing, supervision, funding acquisition.

Declaration of competing interest

The authors declare no conflicts of interest for this article.

Data availability

No data was used for the research described in the article.

Acknowledgements

The authors would like to acknowledge the fruitful discussions within the ELECTRIFIED consortium and the financial support from NWO (Grant No. KICH1.ST01.20.012), Andritz, Avebe, Corbion, Cosun, dsm-firmenich, Meam, The Protein Brewery, and VNP.

Nomenclature

Variables		
A	m^2	Area
C	–	Capacitance
D_i	m^2/s	Diffusivity constant of charged species
$D_{\perp s}$	C/m^2	Electric displacement in sample
$D_{\perp air}$	C/m^2	Electric displacement in air
d	m	Sample thickness
d_{ec}	m	Distance between electrodes
E	V/m	Electric field strength
E_0	V/m	Electric breakdown of air
F_e	N	Electrical force
H_{evap}	kJ/kg	Latent heat of evaporation
h	kJ/K	Heat transfer coefficient
I	A	Current
J	A/m	Current density
k_{cov}	m/s	Convective mass transfer coefficient
L	m	Distance between emitting electrode and sample
N	$mol/m^2/s$	Molar flux
N_{EHD}	–	EHD number
p	Pa	Pressure
P_{adv}	Pa	Pressure at advancing part droplet
P_{rec}	Pa	Pressure at receding part droplet
q	kJ/kg	Heat flux of evaporation
RH	%	Relative humidity
r	m	Cell radius
r_e	m	Curvature radius emitter

(*continued on next page*)

(*continued*)

R_1	m	Radius of curvature advancing part
R_2	m	Radius of curvature receding part
SEC	kJ/kg	Specific energy consumption
T	K	Temperature
u	m/s	Wind velocity
V	V	Electrical potential
V_{interf}	V	Potential material-air interface
V_{wall}	V	Electrical potential on the cell wall at the meniscus interface
y	–	Mole fraction
ϵ_0	–	Permittivity of free space
ϵ_r	–	Relative permittivity of medium
μ	kg/m/s	Fluid viscosity
μ_e	$m^2/V/s$	Mobility of charged species
ν	m^2/s	Kinematic viscosity
ρ_a	kg/m^3	Density of air
ρ_e	C/m^3	Volumetric charge density
ζ	V	Zeta potential
γ_{gl}	J/m^2	Surface tension gas-liquid interface
γ_{SL}	J/m^2	Surface tension solid-liquid interface
γ_0	J/m^2	Surface tension without electric field
Subscripts		
A		Air
F		Food product
W		Water
M		membrane

References

Adamiak, K., & Atten, P. (2004). Simulation of corona discharge in point–plane configuration. *Journal of Electrostatics, 61*(2), 85–98. https://doi.org/10.1016/j.elstat.2004.01.021

Adhikari, B. R., & Khanal, R. (2013). Introduction to the plasma state of matter. *Himalayan Physics, 4*, 60–64.

Alberts, B., Johnson, A., Lewis, J., Morgan, D., Raff, M., Roberts, K., et al. (2015). The plant cell wall. In J. Wilson, & T. Hunt (Eds.), *Molecular biology of the cell* (6th ed.). W.W. Norton & Company. https://doi.org/10.1201/9781315735368.

Alemrajabi, A. A., Rezaee, F., Mirhosseini, M., & Esehaghbeygi, A. (2012). Comparative evaluation of the effects of electrohydrodynamic, oven, and ambient air on carrot cylindrical slices during drying process. *Drying Technology, 30*(1), 88–96. https://doi.org/10.1080/07373937.2011.608913

Babaei, R., Heidarinejad, G., & Pasdarshahri, H. (2018). Performance improvement of EHD-enhanced water evaporation process using optimizing the wire electrode position and the wall-mounted electrode length. *Heat and Mass Transfer, 54*(12), 3785–3796. https://doi.org/10.1007/s00231-018-2404-5

Barbosa-Cánovas, G., & Vega-Mercado, H. (1996). *Dehydration of foods*. Springer Science & Business Media.

Bardy, E., Manai, S., Havet, M., & Rouaud, O. (2016). Drying kinetics comparison of methylcellulose gel versus mango fruit in forced convective drying with and without electrohydrodynamic enhancement. *Journal of Heat Transfer, 138*(8). https://doi.org/10.1115/1.4033390

Bashkir, I., Defraeye, T., Kudra, T., & Martynenko, A. (2020). Electrohydrodynamic drying of plant-based foods and food model systems. *Food Engineering Reviews, 12*(4), 473–497. https://doi.org/10.1007/S12393-020-09229-W/FIGURES/4

Bittencourt, J. A. (2004). *Fundamentals of plasma physics*. Springer Science. https://doi.org/10.1007/978-1-4757-4030-1

Cao, W., Nishiyama, Y., & Koide, S. (2004). Electrohydrodynamic drying characteristics of wheat using high voltage electrostatic field. *Journal of Food Engineering, 62*(3), 209–213. https://doi.org/10.1016/S0260-8774(03)00232-2

Chakraborty, S. (2008). Electrocapillary. In *Encyclopedia of microfluidics and nanofluidics* (1st ed., pp. 460–469). Springer US. https://doi.org/10.1007/978-0-387-48998-8_399.

Chandramohan, P. V. (2020). Convective drying of food materials: An overview with fundamental aspect, recent developments, and summary. *Heat Transfer, 49*(3), 1281–1313. https://doi.org/10.1002/htj.21662

Chang, Y. J., Peng, J. C., Lin, S. C., & Lai, F. C. (2020). Flow induced by an EHD gas pump with secondary emitting electrodes. *Journal of Electrostatics, 105*, Article 103438. https://doi.org/10.1016/j.elstat.2020.103438

Chen, J., & Davidson, J. H. (2002). Ozone production in the positive DC corona discharge: Model and comparison to experiments. *Plasma Chemistry and Plasma Processing, 22*(4), 495–522. https://doi.org/10.1023/A:1021315412208

Defraeye, T., & Martynenko, A. (2018a). Electrohydrodynamic drying of food: New insights from conjugate modeling. *Journal of Cleaner Production, 198*, 269–284. https://doi.org/10.1016/j.jclepro.2018.06.250

Defraeye, T., & Martynenko, A. (2018b). Future perspectives for electrohydrodynamic drying of biomaterials. *Drying Technology, 36*(1), 1–10. https://doi.org/10.1080/07373937.2017.1326130

Di Fraia, S., Massarotti, N., & Nithiarasu, P. (2018). Modelling electro-osmotic flow in porous media: A review. *International Journal of Numerical Methods for Heat and Fluid Flow, 28*(2), 472–497. https://doi.org/10.1108/HFF-11-2016-0437

Dima, P., Gulbinas, G., Stubbe, P. R., Mendes, A. C., & Chronakis, I. S. (2022). Electrohydrodynamic drying of probiotics. *Innovative Food Science and Emerging Technologies, 82*. https://doi.org/10.1016/j.ifset.2022.103201

Ding, C., Lu, J., & Song, Z. (2015). Electrohydrodynamic drying of carrot slices. *PLoS One, 10*(4), Article e0124077. https://doi.org/10.1371/journal.pone.0124077

Dumitran, L. M., Atten, P., Notingher, P. V., & Dascalescu, L. (2006). 2-D corona field computation in configurations with ionising and non-ionising electrodes. *Journal of Electrostatics, 64*(3–4), 176–186. https://doi.org/10.1016/J.ELSTAT.2005.05.005

Esehaghbeygi, A. (2012). Effect of electrohydrodynamic and batch drying on rice fissuring. *Drying Technology, 30*(14), 1644–1648. https://doi.org/10.1080/07373937.2012.701262

Esehaghbeygi, A., & Basiry, M. (2011). Electrohydrodynamic (EHD) drying of tomato slices (Lycopersicon esculentum). *Journal of Food Engineering, 104*(4), 628–631. https://doi.org/10.1016/j.jfoodeng.2011.01.032

European Commission. (2017). *EU air quality standards*.

Fei, J., Ding, B., Koh, S. W., Ge, J., Wang, X., Lee, L., et al. (2021). Mechanistic investigation of electrostatic field-enhanced water evaporation. *Advanced Science, 8*(18). https://doi.org/10.1002/advs.202100875

Frabetti, A. C. C., Garnault, T., Curto, H., Thillier, A., Boillereaux, L., Rouaud, O., et al. (2023). Dielectric properties of low moisture foods measured by open-ended coaxial probe and cavity perturbation technique. *European Food Research and Technology, 249*(11), 2861–2873. https://doi.org/10.1007/s00217-023-04333-7

Gargano, S., Lirer, S., & Flora, A. (2022). Relative relevance of factors affecting the electrokinetic dewatering of soft clayey soils. *Proceedings of the Institution of Civil Engineers - Ground Improvement, 175*(2), 127–138. https://doi.org/10.1680/jgrim.20.00023

Glockner, P. S., & Naterer, G. F. (2006). Surface tension and frictional resistance of thermocapillary pumping in a closed microchannel. *International Journal of Heat and Mass Transfer, 49*(23–24), 4424–4436. https://doi.org/10.1016/j.ijheatmasstransfer.2006.05.005

Golberg, A., & Rubinsky, B. (2013). Mass transfer phenomena in electroporation. In *Transport in biological media* (pp. 455–492). Elsevier. https://doi.org/10.1016/B978-0-12-415824-5.00012-6.

Golsefid, S. S. M., Amanifard, N., Deylami, H. M., & Dolati, F. (2017). Numerical and experimental study on EHD heat transfer enhancement with Joule heating effect through a rectangular enclosure. *Applied Thermal Engineering, 123*, 689–698. https://doi.org/10.1016/J.APPLTHERMALENG.2017.05.129

Granados, V. H., Pinheiro, M. J., & Sá, P. A. (2016). Electrostatic propulsion device for aerodynamics applications. *Physics of Plasmas, 23*(7). https://doi.org/10.1063/1.4958815

Huang, M., & Lai, F. C. (2010). Numerical study of EHD-enhanced water evaporation. *Journal of Electrostatics, 68*(4), 364–370. https://doi.org/10.1016/J.ELSTAT.2010.05.003

Icier, F., & Baysal, T. (2004). Dielectrical properties of food materials—1: Factors affecting and industrial uses. *Critical Reviews in Food Science and Nutrition, 44*(6), 465–471. https://doi.org/10.1080/10408690490886692

Iranshahi, K., Martynenko, A., & Defraeye, T. (2020). Cutting-down the energy consumption of electrohydrodynamic drying by optimizing mesh collector electrode. *Energy, 208*, Article 118168. https://doi.org/10.1016/j.energy.2020.118168

Iranshahi, K., Onwude, D. I., Martynenko, A., & Defraeye, T. (2022). Dehydration mechanisms in electrohydrodynamic drying of plant-based foods. *Food and Bioproducts Processing, 131*, 202–216. https://doi.org/10.1016/j.fbp.2021.11.009

Iranshahi, K., Onwude, D. I., Rubinetti, D., Martynenko, A., & Defraeye, T. (2022). *Scalable electrohydrodynamic drying configuration for dehydrating biological materials at industrial scale. Unpublished*.

Jewell-Larsen, N. E., Karpov, S. V., Krichtafovitch, I. A., Jayanty, V., Hsu, C.-P., & Mamishev, A. V. (2008). *Modeling of corona-induced electrohydrodynamic flow with.* COMSOL multiphysics.

Jin, X., van Boxtel, A. J. B., Gerkema, E., Vergeldt, F. J., Van As, H., van Straten, G., et al. (2012). Anomalies in moisture transport during broccoli drying monitored by MRI? *Faraday Discussions, 158*, 65. https://doi.org/10.1039/c2fd20049j

Kaptsov, N. A. (1947). *Elektricheskie yavleniya v gazakh i vakuume.* Moscow: OGIZ.

Lai, F. C. (2010). A prototype of EHD-enhanced drying system. *Journal of Electrostatics, 68*(1), 101–104. https://doi.org/10.1016/J.ELSTAT.2009.08.002

Lai, F. C., & Lai, K. W. (2007). EHD-Enhanced drying with wire electrode. *Drying Technology, 20*(7), 1393–1405. https://doi.org/10.1081/DRT-120005858

Lai, F. C., & Sharma, R. K. (2005). EHD-Enhanced drying with multiple needle electrode. *Journal of Electrostatics, 63*(3–4), 223–237. https://doi.org/10.1016/j.elstat.2004.10.004

Lee, J., & Chang-Jin Kim, C.-J. (2000). Surface-tension-driven microactuation based on continuous electrowetting. *Journal of Microelectromechanical Systems, 9*(2), 171–180. https://doi.org/10.1109/84.846697

Lee, Y., Kim, Y.-S., Han, B., Kim, Y.-J., & Kim, H.-J. (2022). Minimizing the size and ozone emission of electrostatic precipitators using dielectric and rolled carbon film coatings. *IEEE Transactions on Industry Applications, 58*(1), 753–759. https://doi.org/10.1109/TIA.2021.3122402

Lee, J. R., & Lau, E. Von (2017). Effects of relative humidity in the convective heat transfer over flat surface using ionic wind. *Applied Thermal Engineering, 114*, 554–560. https://doi.org/10.1016/j.applthermaleng.2016.12.030

Leu, J.-S., Jang, J.-Y., & Wu, Y.-H. (2020). Three-dimensional electrohydrodynamic enhanced water evaporation using needle-arrayed electrodes. *Heat Transfer Engineering, 41*(22), 1921–1937. https://doi.org/10.1080/01457632.2019.1675250

Lewicki, P. P. (2006). Design of hot air drying for better foods. *Trends in Food Science & Technology, 17*(4), 153–163. https://doi.org/10.1016/j.tifs.2005.10.012

Li, Y., Yu, X., Zhang, S., & Zhang, Y. (2021). Influences of K+, Ca2+, and Al3+ on electrokinetic process and conductive mechanism of sludge electro-dewatering. *Environmental Research, 198*, Article 111222. https://doi.org/10.1016/j.envres.2021.111222

Lillard, R. S., & Pint, B. A. (2020). Principles of corrosion in nuclear systems: Theory and analytical methods. In *Comprehensive nuclear materials* (pp. 1–32). Elsevier. https://doi.org/10.1016/B978-0-12-803581-8.11761-8.

Liu, J., Wu, J., Zhou, X., Liu, C., & Wei, Y. (2022). Impact of process parameters and sludge properties on electro-dewatering performance. *Drying Technology, 40*(1), 213–225. https://doi.org/10.1080/07373937.2020.1806864

Liu, C., Yu, D., Kirk, D. W., & Xu, Y. (2016). Porous silicon carbide derived from apple fruit with high electromagnetic absorption performance. *Journal of Materials Chemistry C, 4*(23), 5349–5356. https://doi.org/10.1039/C6TC01319H

Martynenko, A., Astatkie, T., & Defraeye, T. (2020). The role of convection in electrohydrodynamic drying. *Journal of Food Engineering, 271*, Article 109777. https://doi.org/10.1016/j.jfoodeng.2019.109777

Martynenko, A., Astatkie, T., Riaud, N., Wells, P., & Kudra, T. (2017). Driving forces for mass transfer in electrohydrodynamic (EHD) drying. *Innovative Food Science & Emerging Technologies, 43*, 18–25. https://doi.org/10.1016/j.ifset.2017.07.022

Martynenko, A., Bashkir, I., & Kudra, T. (2019). Electrically enhanced drying of white champignons. *Drying Technology, 39*(2), 234–244. https://doi.org/10.1080/07373937.2019.1670672

Martynenko, A., Bashkir, I., & Kudra, T. (2021). The energy efficiency of electrohydrodynamic (EHD) drying of foods. *Trends in Food Science & Technology, 118*, 744–764. https://doi.org/10.1016/j.tifs.2021.09.002

Martynenko, A., Iranshahi, K., & Defraeye, T. (2022). Plate versus mesh collecting electrode for electrohydrodynamic (EHD) drying. *Drying Technology, 40*(13), 2759–2769. https://doi.org/10.1080/07373937.2021.1962338

Martynenko, A., & Kudra, T. (2020). Electrohydrodynamic dryer: Effect of emitters' density and gap between discharge and collecting electrodes. *Drying Technology, 38*(1–2), 158–167. https://doi.org/10.1080/07373937.2019.1621338

Martynenko, A., & Misra, N. N. (2021). Thermal phenomena in electrohydrodynamic (EHD) drying. *Innovative Food Science & Emerging Technologies, 74*, Article 102859. https://doi.org/10.1016/J.IFSET.2021.102859

Martynenko, A., & Zheng, W. (2016). Electrohydrodynamic drying of apple slices: Energy and quality aspects. *Journal of Food Engineering, 168*, 215–222. https://doi.org/10.1016/j.jfoodeng.2015.07.043

Meng, Z., Cui, X., Liu, Y., Hu, R., Du, C., Wang, S., et al. (2022). Drying characteristics of banana slices under heat pump-electrohydrodynamic (EHD) combined drying. *Sustainable Energy Technologies and Assessments, 54*, Article 102907. https://doi.org/10.1016/j.seta.2022.102907

Moreau, E., Audier, P., & Benard, N. (2018). Ionic wind produced by positive and negative corona discharges in air. *Journal of Electrostatics, 93*, 85–96. https://doi.org/10.1016/J.ELSTAT.2018.03.009

Moučka, R., Sedlačík, M., & Pátíková, Z. (2023). Fractional viscoelastic models of porcine skin and its gelatin-based surrogates. *Mechanics of Materials, 177*, Article 104559. https://doi.org/10.1016/j.mechmat.2023.104559

Mushyam, A., Rodrigues, F., & Pascoa, J. C. (2019). A plasma-fluid model for EHD flow in DBD actuators and experimental validation. *International Journal for Numerical Methods in Fluids, 90*(3), 115–139. https://doi.org/10.1002/fld.4714

Ni, J., Ding, C., Zhang, Y., Song, Z., Hu, X., & Hao, T. (2019). Electrohydrodynamic drying of Chinese wolfberry in a multiple needle-to-plate electrode system. *Foods, 8*(5), 152. https://doi.org/10.3390/FOODS8050152

Nicholas, N., & Abuzairi, T. (2019). Electrohydrodynamic drying process of the amoxicillin powder using a high direct current (DC) voltage. *AIP Conference Proceedings, 2193*(1), Article 050012. https://doi.org/10.1063/1.5139385

O'Brien, R. W. (1986). Electroosmosis in porous materials. *Journal of Colloid and Interface Science, 110*(2), 477–487. https://doi.org/10.1016/0021-9797(86)90401-7

Onwude, D. I., Iranshahi, K., Rubinetti, D., Martynenko, A., & Defraeye, T. (2021). Scaling-up electrohydrodynamic drying for energy-efficient food drying via physics-based simulations. *Journal of Cleaner Production, 329*. https://doi.org/10.1016/j.jclepro.2021.129690

Park, S., Cvelbar, U., Choe, W., & Moon, S. Y. (2018). The creation of electric wind due to the electrohydrodynamic force. *Nature Communications, 9*(1), 1–8. https://doi.org/10.1038/s41467-017-02766-9

Paul, A., Astatkie, E., & Martynenko, A. (2022). Electrohydrodynamic drying of fruit slices: Effect on drying kinetics, energy consumption, and product quality. *Journal of Food Processing and Preservation, 46*(10). https://doi.org/10.1111/jfpp.16812

Paul, A., & Martynenko, A. (2022). The effect of material thickness, load density, external airflow, and relative humidity on the drying efficiency and quality of EHD-dried apples. *Foods, 11*(18). https://doi.org/10.3390/foods11182765

Peek, F. W. (2017). *Dielectric phenomena in high voltage engineering.* Creative Media Partners, LLC.

Raghavan, G. S. V., Rennie, T. J., Sunjka, P. S., Orsat, V., Phaphuangwittayakul, W., & Terdtoon, P. (2005). Overview of new techniques for drying biological materials with emphasis on energy aspects. *Brazilian Journal of Chemical Engineering, 22*(2), 195–201. https://doi.org/10.1590/S0104-66322005000200005

Rezinkina, M., Rezinkin, O., D'Alessandro, F., Danyliuk, A., Guchenko, A., & Lytvynenko, S. (2017). Experimental and modelling study of the dependence of corona discharge on electrode geometry and ambient electric field. *Journal of Electrostatics, 87*, 79–85. https://doi.org/10.1016/j.elstat.2017.03.008

Robinson, M. (2013). Movement of air in the electric wind of the corona discharge. *Transactions of the American Institute of Electrical Engineers, Part I: Communication and Electronics, 80*(2), 143–150. https://doi.org/10.1109/TCE.1961.6373091

Rubinetti, D., Iranshahi, K., Onwude, D. I., Nicolaï, B. M., Xie, L., & Defraeye, T. (2024). Energy-saving discharge needle shape for electrohydrodynamic airflow generation. *Journal of Electrostatics, 127*, Article 103876. https://doi.org/10.1016/J.ELSTAT.2023.103876

Rubinsky, B., Onik, G., & Mikus, P. (2007). Irreversible electroporation: A new ablation modality — clinical implications. *Technology in Cancer Research and Treatment, 6*(1), 37–48. https://doi.org/10.1177/153303460700600106

Saneewong Na Ayuttaya, S., Chaktranond, C., Rattanadecho, P., & Kreewatcharin, T. (2012). Effect of ground arrangements on swirling flow in a rectangular duct subjected to electrohydrodynamic effects. *Journal of Fluids Engineering, Transactions of the ASME, 134*(5). https://doi.org/10.1115/1.4006699

Shrotriya, V., & Yang, Y. (2005). Capacitance–voltage characterization of polymer light-emitting diodes. *Journal of Applied Physics, 97*(5). https://doi.org/10.1063/1.1857053

Sridhar, A., Vaishampayan, V., Senthil Kumar, P., Ponnuchamy, M., & Kapoor, A. (2022). Extraction techniques in food industry: Insights into process parameters and their optimization. *Food and Chemical Toxicology, 166*, Article 113207. https://doi.org/10.1016/j.fct.2022.113207

Stone, H. A., Stroock, A. D., & Ajdari, A. (2004). Engineering flows in small devices: Microfluidics toward a lab-on-a-chip. *Annual Review of Fluid Mechanics, 36*(1), 381–411. https://doi.org/10.1146/annurev.fluid.36.050802.122124

Stuetzer, O. M. (1959). Ion drag pressure generation. *Journal of Applied Physics, 30*(7), 984–994. https://doi.org/10.1063/1.1777003

Suvanjumrat, C., Chuckpaiwong, I., Chookaew, W., & Priyadumkol, J. (2024). Assessment of the pineapple drying with a forced convection solar-electrohydrodynamic dryer. *Case Studies in Thermal Engineering, 59*, Article 104582. https://doi.org/10.1016/j.csite.2024.104582

Taghavi Fadaki, S. S., Amanifard, N., Deylami, H. M., & Dolati, F. (2017). Numerical analysis of the EHD driven flow with heat transfer in a smooth channel using multiple collectors. *Heat and Mass Transfer, 53*(7), 2445–2460. https://doi.org/10.1007/s00231-017-1994-7

Taghian Dinani, S., Havet, M., Hamdami, N., & Shahedi, M. (2014). Drying of mushroom slices using hot air combined with an electrohydrodynamic (EHD) drying system. *Drying Technology, 32*(5), 597–605. https://doi.org/10.1080/07373937.2013.851086

Tippayawong, N., Tantakitti, C., & Thavornun, S. (2008). Energy efficiency improvements in longan drying practice. *Energy, 33*(7), 1137–1143. https://doi.org/10.1016/j.energy.2008.02.007

Tıraş, B., Dede, S., & Altay, F. (2019). Dielectric properties of foods. *Turkish Journal of Agriculture - Food Science and Technology, 7*(11), 1805–1816. https://doi.org/10.24925/turjaf.v7i11.1805-1816.2650

Vaessen, E. M. J., den Besten, H. M. W., Leito, K. M. N., & Schutyser, M. A. I. (2020). Pulsed electric field pre-treatment for enhanced bacterial survival after drying: Effect of carrier matrix and strain variability. *Innovative Food Science & Emerging Technologies, 66*, Article 102515. https://doi.org/10.1016/j.ifset.2020.102515

Wall, S. (2010). The history of electrokinetic phenomena. *Current Opinion in Colloid & Interface Science, 15*(3), 119–124. https://doi.org/10.1016/j.cocis.2009.12.005

Wang, J., Cai, R., Zhu, T., & Liu, Y. (2022). Ionic wind intensity enhancement and ozone reduction in a solid-state fan via electromagnetic field action. *Plasma Chemistry and Plasma Processing, 42*(5), 1045–1067. https://doi.org/10.1007/s11090-022-10273-z

Wang, Y., & Ding, C. (2023). Effect of electrohydrodynamic drying on drying characteristics and physicochemical properties of carrot. *Foods, 12*(23), 4228. https://doi.org/10.3390/foods12234228

Wang, J., Zhu, T., Cai, Y. xi, Zhang, J. fei, & Wang, J. bo (2020). Review on the recent development of corona wind and its application in heat transfer enhancement. *International Journal of Heat and Mass Transfer, 152*, Article 119545. https://doi.org/10.1016/j.ijheatmasstransfer.2020.119545

Wu, S., Xu, Z., Tian, S., Luo, T., & Xiong, G. (2022). Enhanced water evaporation under spatially gradient electric fields: A molecular dynamics study. *Journal of Molecular Liquids, 360*, Article 119410. https://doi.org/10.1016/J.MOLLIQ.2022.119410

Xie, Z., Hao, S., Wang, W., Kou, J., & Fan, J. (2022). Electric field direction-induced gas/water selectively entering nanochannel. *Journal of Molecular Liquids, 363*, Article 119852. https://doi.org/10.1016/J.MOLLIQ.2022.119852

Xu, H., Wang, J., Tian, J., Huo, Y., Li, B., Wang, D., et al. (2021). Evaporation characteristics and heat transfer enhancement of sessile droplets under non-uniform electric field. *Experimental Thermal and Fluid Science, 126*, Article 110378. https://doi.org/10.1016/J.EXPTHERMFLUSCI.2021.110378

Xu, C., Xu, Y., Wang, J., Qiu, S., Rao, B., & Xu, P. (2023). A pore-scale physical model for electric dewatering of municipal sludge based on fractal geometry. *Journal of Environmental Engineering, 149*(3). https://doi.org/10.1061/JOEEDU.EEENG-7089

Xu, X., Zhang, Y., & Sun, L. (2018). Transport mechanism by which droplets on electrowetting-on-dielectric devices. *Chinese Journal of Physics, 56*(6), 2887–2896. https://doi.org/10.1016/j.cjph.2018.09.024

Yang, M., & Yagoobi, J. (2022). Enhancement of drying rate of moist porous media with dielectrophoresis mechanism. *Drying Technology, 40*(14), 2952–2963. https://doi.org/10.1080/07373937.2021.1981922

Zeng, M. J., Qu, Z. G., & Zhang, J. F. (2023). Negative corona discharge and flow characteristics of a two-stage needle-to-ring configuration ionic wind pump for temperature and relative humidity. *International Journal of Heat and Mass Transfer, 201*, Article 123561. https://doi.org/10.1016/J.IJHEATMASSTRANSFER.2022.123561

Zhang, Q., Cui, G., He, X., Wang, Z., Tang, T., Zhao, Q., et al. (2022). Effects of voltage and pressure on sludge electro-dewatering process and the dewatering mechanisms investigation. *Environmental Research, 212*, Article 113490. https://doi.org/10.1016/j.envres.2022.113490

Zheng, D. J., Liu, H. J., Cheng, Y. Q., & Li, L. T. (2011). Electrode configuration and polarity effects on water evaporation enhancement by electric field. *International Journal of Food Engineering, 7*(2). https://doi.org/10.2202/1556-3758.1794